

Carbon Dots Decorated Hierarchical NiCo₂S₄/Ni₃S₂ Composite for Efficient Water Splitting

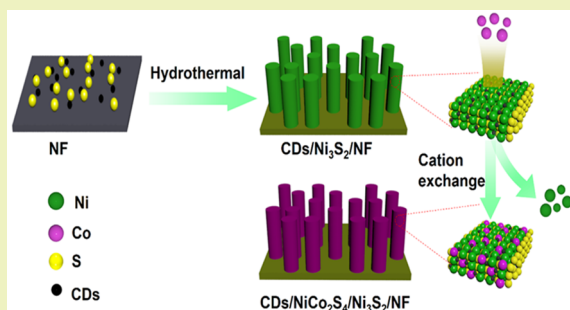
Xinyu Zhao, Hui Liu,^{1D} Yuan Rao,^{1D} Xinxin Li, Jialin Wang, Guangsen Xia, and Mingbo Wu^{*1D}

State Key Laboratory of Heavy Oil Processing, Institute of New Energy, College of Chemical Engineering, China University of Petroleum (East China), Qingdao 266580, People's Republic of China

Supporting Information

ABSTRACT: The decomposition of water into hydrogen and oxygen is an effective method to generate new energy. How to develop highly efficient catalysts with low cost for the hydrolysis of water is a huge challenge. Herein, heterogeneous CDs/NiCo₂S₄/Ni₃S₂ nanorods were constructed on nickel foam (CDs/NiCo₂S₄/Ni₃S₂/NF) by Co ion exchange on carbon dots (CDs) and sulfur codoped nickel foam (NF). The designed CDs/NiCo₂S₄/Ni₃S₂/NF as a self-standing electrocatalyst shows excellent electrocatalytic properties. In the hydrogen evolution reaction process, the current density can reach 10 mA cm⁻² only with the overpotential of 0.127 V. During the oxygen evolution reaction process, overpotential of 0.116 V is enough to achieve the same current density. Meanwhile, the CDs/NiCo₂S₄/Ni₃S₂/NF electrode can serve as both anode and cathode in alkaline electrolyte, and overpotential of 1.50 V can drive the overall water splitting with superior durability. Such excellent properties are mainly due to (1) a large number of exposed active sites provided by carbon dots modified transition metal chalcogenide (NiCo₂S₄ and Ni₃S₂), (2) the changed electronic structure caused by the incorporation of carbon dots and Co ions and the synergistic effect between NiCo₂S₄ and Ni₃S₂, (3) the accelerated electron transfer and mass transfer processes owing to the hierarchical structure formed by 3D nickel foam and one-dimensional CDs/NiCo₂S₄/Ni₃S₂/NF nanorods. This study can facilitate with the production of efficient and non-noble metal catalysts for overall water splitting.

KEYWORDS: Carbon dots, Transition metal chalcogenides, Hydrogen evolution reaction, Oxygen evolution reaction, Water splitting



INTRODUCTION

With the rapid development of our societies, the need for energy is rising sharply. Meanwhile, the limited reservation of conventional fossil energies and the increasingly severe environmental contamination require development of new energy resources that are effective and environmental friendly.¹ As a kind of “green energy” with abundant resources, high effectiveness and no secondary pollution, hydrogen energy is considered as one of the ideal energy sources to solve the energy and environmental crises in the postfossil era.² Electrolysis of water is one reliable way to produce hydrogen, during which nonstorable renewable resources (such as solar energy, wind energy, tidal energy, and so on) can be used to generate electricity for electrolyzing water. The electrolyzed water can not only produce hydrogen and oxygen with high purity, but also can store the electric energy into chemical energy for further utilization.³ However, electrolyzed water is thermodynamically nonspontaneous adverse reaction, requiring a high overpotential for oxygen evolution reaction (OER) and hydrogen evolution reaction (HER) to provide a seemly reaction rate.^{4–6} In order to scale up the hydrogen production, it is necessary to reduce the reaction potential and improve the reaction rate. Thus, the development of efficient and resource-rich catalysts for water electrolysis becomes an urgent issue.

Now, platinum group precious metals are commercially used as catalysts for water splitting, but these catalysts are in less reserve and expensive, making them fail to meet the real needs of large-scale production.^{7,8} Therefore, in recent years, many researchers have devoted themselves to the design and development of new catalysts with high efficiency and low cost.

So far, Fe-, Co-, or Ni-based transition metal chalcogenides (TMCs) materials, for example, Mo–S,^{16–18} Ni–S,^{19–23} Mo–Se,²⁴ Co–Se²⁵ and Co–S,^{26–28} have been found can be catalytic activity sites on both HER and OER.^{9–15} As a typical kind of transition metal chalcogenides, Ni–S materials have different stoichiometric ratios, such as Ni₃S₂,¹⁹ NiS₂²¹ and NiS,²¹ and different morphologies, including nanorods,²⁰ nanoparticles,²¹ nanosheets¹⁹ and nanowires.²⁹ They were reported as effective electrocatalysts. Nevertheless, these catalysts have good performance in single reaction. When they are used as bifunctional catalyst, their catalytic performance is significantly lower than standard electrocatalysts. Fortunately, TMCs compounds have been proved feasible catalysts. For example, Gao et al. prepared MoS₂–Ni₃S₂

Received: November 1, 2018

Revised: November 27, 2018

Published: December 28, 2018

heteronanorods via a hydrothermal method, which show good water splitting performance.³⁰ Feng et al. also improved electrocatalytic activity by preparing MoS₂/Ni₃S₂ heterostructures.³¹ In addition, Zou et al. prepared Ni_xCo_{3-x}S₄/Ni₃S₂ nanosheets with excellent electrocatalytic performance and stability through the introduction of Co ions.³² The electrocatalytic performance can be improved by the synergistic effect among TMCs compound. Nevertheless, it is still difficult to construct efficient electrocatalyst with subtly integrated structure by feasible methods. Cation exchange is versatile and has been used in producing various sulfide nanomaterials.³⁸

In order to further improve the performance of the catalyst, different forms of nanocarbon materials were coupled with electrocatalysts to improve the catalytic performance.^{33,34} Carbon dots (CDs) with diameter less than 10 nm are the newest members of carbon material family.³⁵ When CDs are employed, there will have large space to improve the catalysis performance of TMCs-carbon materials. This is out of the reason that CDs are 0D nanoparticles with natural merits. On the one hand, compared with those multidimensional carbon materials, CDs are more flexible for forming different structures. On the other hand, when CDs and TMCs assemble together, there will be more active sites exposed. What is more important is that, with the highest specific surface area, CDs can carry more organic groups. This can contribute to the surface wettability. In this way, larger interface area between CDs, TMCs, as well as electrolytes for electrochemical reactions can be formed.³⁶ All these merits can ensure a promising future of CDs-TMCs composites in the area of electrocatalyst. Under such inspiration, the preparation of electrocatalyst from CDs modified TMCs via cation exchange was developed to improve catalysis performance. Herein, we designed a new type of material by using a one-step hydrothermal method to grow CDs/Ni₃S₂ nanorods on nickel foam as precursors, and introducing Co atoms through cation exchange to form a highly efficient CDs/NiCo₂S₄/Ni₃S₂ electrode with heteronanorods structure. As it is expected, CDs/NiCo₂S₄/Ni₃S₂/NF shows high catalytic activity, outperforming most reported catalysts based on non-noble-metal for water splitting.

EXPERIMENTAL SECTION

Synthesis of CDs/Ni₃S₂/NF. Synthesis of CDs was carried out in accordance with the reported method.³⁷ CDs/Ni₃S₂/NF nanorods were then synthesized by hydrothermal method. The purchased foam nickel (thickness 1.5 mm) was ultrasonically washed with acetone, hydrogen chloride, ethanol and deionized water for 20 min, respectively. Next, it should be dried at 60 °C for 1 h. Then a piece of foam nickel (1 cm × 4 cm) was immersed into a 50 mL Teflon-lined stainless autoclave containing 4 mol thiourea and 30 mL of 1.0 mg mL⁻¹ carbon dots solution. The autoclave was sealed and kept at 180 °C for 3 h in a rotary oven. Then, it was cooled at the room temperature naturally and was washed by deionized water and absolute ethanol for three times repeatedly and was dried in a vacuum oven at 60 °C for 12 h to obtain CDs/Ni₃S₂/NF nanorods. In contrast, the synthesis of Ni₃S₂/NF requires only the replacement of CDs solution with deionized water under the same conditions.

Synthesis of CDs/NiCo₂S₄/Ni₃S₂/NF. The preparation of CDs/NiCo₂S₄/Ni₃S₂/NF was conducted through cation exchange reaction between CDs/Ni₃S₂/NF and Co ions. CDs/Ni₃S₂/NF was immersed into a 50 mL Teflon-lined stainless autoclave that contained ethylene glycol (30 mL) and cobaltous acetate tetrahydrate (2.5 mmol). After that, at 200 °C, it was sealed and placed in a rotating oven for 12 h. The obtained sample was washed with deionized water and anhydrous

ethanol repeatedly and dried in a vacuum oven overnight to obtain CDs/NiCo₂S₄/Ni₃S₂/NF. For comparison, the TMCs without carbon dots (NiCo₂S₄/Ni₃S₂/NF) was prepared. For NiCo₂S₄/Ni₃S₂/NF, the loading mass was about 4 mg cm⁻². This number was obtained by accurate weighing of the analytical balance before and after hydrothermal treatment.

Materials Characterizations. The X-ray diffraction patterns (XRD) were recorded on a PANalytical X-ray Diffractometer (Cu K α) with a 2 θ range from 10° to 70°. The Raman spectra were recorded on a Raman spectrometer of Renishaw. The X-ray photoelectron spectroscopy (XPS) spectra were recorded on a ESCALAB 250XI X-ray spectrometer with Al as a photo source. All XPS curves were fitted and background subtracted. Scanning electron microscopy (SEM) measurements were performed on a ZEISS MERLIN. Transmission electron microscopy (TEM) characterizations were performed on a JEM2100 F scanning transmission electron microscopy. The obtained self-supporting electrode was directly used in electrochemical performance characterization.

Electrochemical Measurements. All the electrochemical measurements were performed on a CHI 760E (CHI Instruments, Shanghai) electrochemical analyzer in a standard three-electrode system. The obtained CDs/NiCo₂S₄/Ni₃S₂/NF served as working electrode, a carbon rod was used as the counter electrode, and an Ag/AgCl electrode was used as the reference electrode in 1.0 M KOH solution. In this study, all shown potentials were calibrated to RHE according to the equation: $E(\text{RHE}) = E(\text{Ag}/\text{AgCl}) + (0.197 \text{ V}) + 0.059 \text{ pH}$. The scanning rate of 5 mV/s for linear sweep voltammetry (LSV) measurements was tested from 0 to 0.8 V. There was no activation before the polarization curves had been recorded. After that, the LSV curves did not go through iR correction. Chronoamperometric measurements were used to get the durabilities of obtained materials. As a comparison, we prepared the Pt/C (20 wt %) and RuO₂ drop coating on NF, and they were used as working electrodes. The following is the typical procedure: (1) 10 μL of Nafion (5 wt %) solution and the 4 mg of Pt/C or RuO₂ were dispersed in 800 μL of anhydrous ethanol by sonication for 60 min. (2) 320 μL of this solution was dropped onto NF (1 cm × 0.6 cm) in order to make sure that the compared electrode has the same working area of CDs/NiCo₂S₄/Ni₃S₂/NF and the same loading amount of 4 mg cm⁻². (3) In order to avoid the covering materials from falling off, 80 μL of Nafion (0.5 wt %) solution dissolved in ethanol was drop-cast on the surface of the electrode. After that, it was dried in an electric heater.

RESULTS AND DISCUSSION

Through the method of cation exchange, we successfully prepared CDs/NiCo₂S₄/Ni₃S₂/NF nanorods and the synthesis of CDs/NiCo₂S₄/Ni₃S₂/NF is illustrated schematically in Scheme 1. First, CDs/Ni₃S₂/NF were hydrothermally prepared by the carbon dots induction method. After that, the obtained CDs/Ni₃S₂/NF nanorods precursors and Co ions were subjected to cation exchange reaction at 200 °C, which

Scheme 1. Schematic Preparation of 3D CDs/NiCo₂S₄/Ni₃S₂/NF



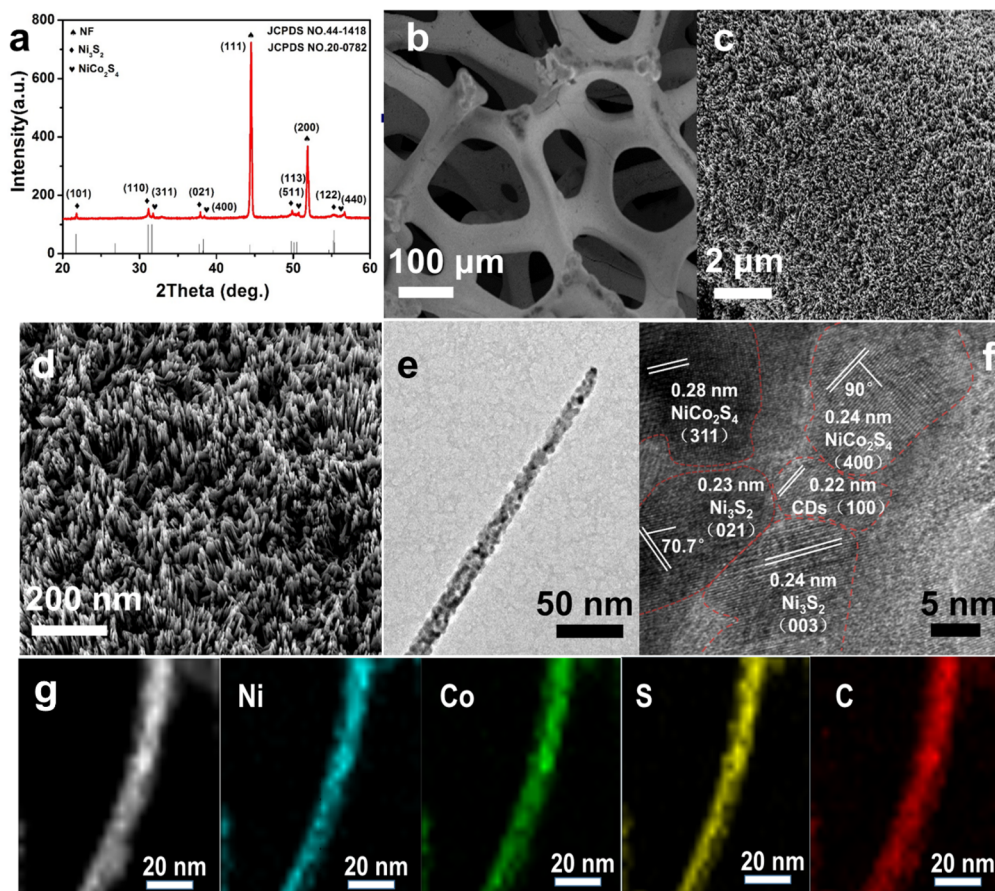


Figure 1. (a) XRD pattern of CDs/NiCo₂S₄/Ni₃S₂/NF. (b, c and d) SEM images of CDs/NiCo₂S₄/Ni₃S₂/NF. (e) TEM and (f) high-resolution transmission electron microscopy (HRTEM) images of CDs/NiCo₂S₄/Ni₃S₂/NF nanorods. (g) STEM images and the corresponding EDX elemental mapping images of Ni, Co, S and C taken from CDs/NiCo₂S₄/Ni₃S₂/NF nanorods.

produced the CDs/NiCo₂S₄/Ni₃S₂/NF nanorods. Here, the synthesis of CDs/Ni₃S₂ with exposed (021) crystal face is based on our previous work.³⁷ The transmission electron microscopy (TEM) images and X-ray diffraction (XRD) pattern of CDs are provided in Figure S1a,b (see Supporting Information). The XRD pattern reveals a much greater diffraction peak centered at 25.7°, which is a characteristic peak of a typical carbon material. In addition, from the TEM image, it can be seen that the distribution of synthesized CDs is relatively homogeneous, and the 0.22 nm lattice spacing shown in the high-resolution TEM (HRTEM) image of CDs also corresponds well to that of graphitic carbon (100) plane. The FT-IR spectra (Figure S1c) demonstrates the existence of various functional groups on CDs. It is obviously different from petroleum coke. Raman spectra (Figure S1d) of petroleum coke and CDs further indicate typical D and G bands of carbon materials. These results clearly indicate the successful formation of CDs. The SEM image (Figure S2) show the growth process of Ni₃S₂ nanorods with different morphologies. It can be seen that after 1 h reaction at 180 °C, nucleation started on the surface of nickel foam and gradually grew with the continuation of the reaction. The phenomenon of transition growth occurred in after 4 h of the reaction, and nanorods began to gather together. In this experiment, we chose the uniformly distributed CDs/Ni₃S₂/NF rod-like structure obtained after 3 h of reaction as a precursor, and then proceeded to the next ion exchange reaction. This reaction can not only maintain the morphology of the

precursor well, but also introduce heteroatoms to form heterogeneous surfaces. A comparative experiment was also conducted in the similar condition without adding carbon dots. From the SEM image (Figure S3b), the obvious nanosphere-like structure can be seen, which is obviously different from the rod-like structure formed after carbon dots were added.

Moreover, by the X-ray diffraction (XRD) pattern, it was confirmed that the nanorods belong to NiCo₂S₄, Ni₃S₂ and CDs. As shown in Figure 1a, the diffraction peaks at 31.6, 38.3, 50.5 and 55.3° can be assigned to (311), (400), (511) and (440) planes of the cubic NiCo₂S₄ phase (JCPDS card No. 20-0782), respectively, and the peaks at 21.8, 31.1, 38.3, 49.7 and 55.1° corresponding to (101), (110), (021), (113) and (122) planes of rhombohedral Ni₃S₂ (JCPDS card No. 44-1418), respectively.^{19,32} What is more, at 44.5 and 51.8°, the two peaks shown were metallic Ni foam (JCPDS card No. 04-0850). All these showed that successful preparation of CDs/NiCo₂S₄/Ni₃S₂/NF after cation exchange reaction between CDs/Ni₃S₂ and cobalt ions. For comparison, NiCo₂S₄/Ni₃S₂/NF were made by a similar process to that of the preparation of CDs/NiCo₂S₄/Ni₃S₂/NF. The XRD patterns show the formation of NiCo₂S₄/Ni₃S₂/NF (Figure S3a). NiCo₂S₄/Ni₃S₂/NF presents nanosphere morphology (Figure S3b) rather than the aligned nanorods architecture of CDs/NiCo₂S₄/Ni₃S₂/NF. The typical scanning electron microscopy (SEM) images of CDs/NiCo₂S₄/Ni₃S₂/NF demonstrate that the material has a three-dimensional porous structure (Figure 1b). In Figure 1c,d, it can be clearly seen that a uniform layer

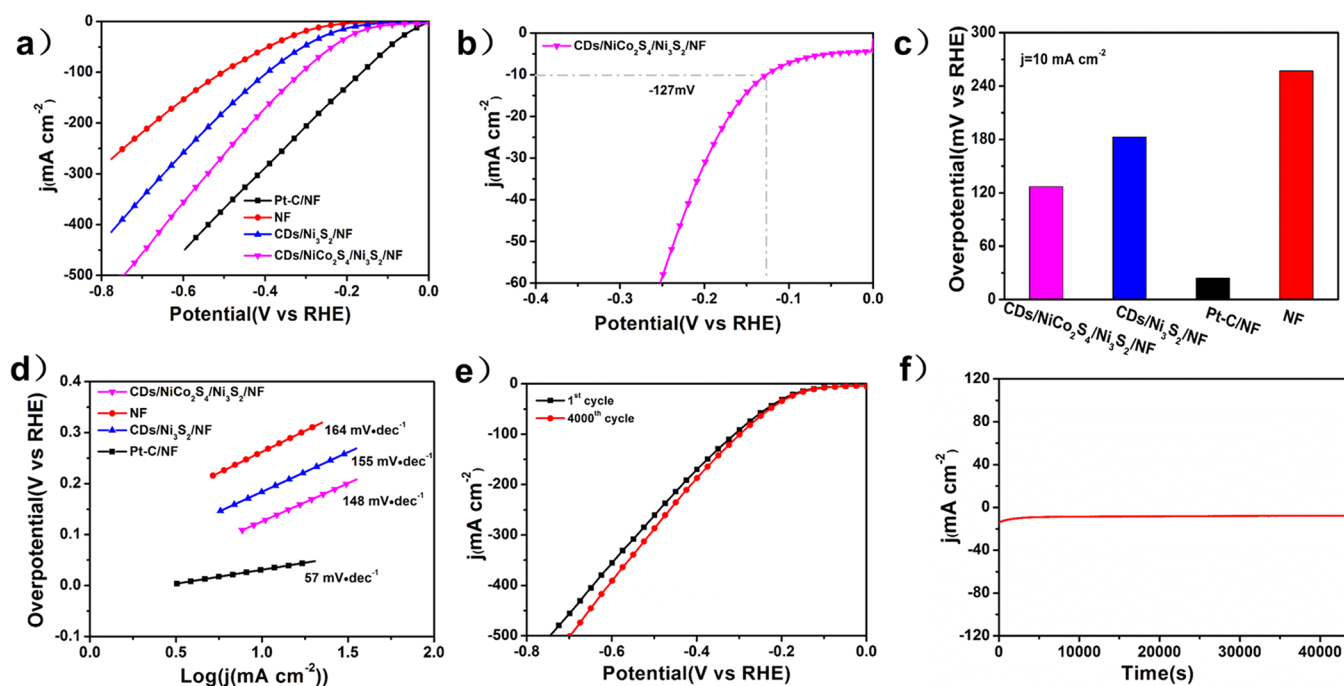


Figure 2. (a) LSV curves of CD/NiCo₂S₄/Ni₃S₂/NF, CD/Ni₃S₂/NF, bare Ni foam and Pt–C/NF. (b) LSV curve of CD/NiCo₂S₄/Ni₃S₂/NF. (c) Overpotential histogram of CD/NiCo₂S₄/Ni₃S₂/NF, CD/Ni₃S₂/NF, bare Ni foam and Pt–C/NF. (d) Tafel plots of CD/NiCo₂S₄/Ni₃S₂/NF, CD/Ni₃S₂/NF, bare Ni foam and Pt–C/NF. (e) LSV curves for CD/NiCo₂S₄/Ni₃S₂/NF before and after potential sweeps between 0 and –0.8 V for 4000 cycles. (f) 12 h chronoamperometry (at a static overpotential of 127 mV) of CD/NiCo₂S₄/Ni₃S₂/NF.

of nanorod structure with length of 50–200 nm covers the surface of the nickel foam skeleton. In order to further prove that the synthesized structure was nanorod, TEM analysis was conducted and the nanorod structure of the material can also be clearly seen in Figure 1e. This indicates that the material can maintain the morphology of the precursor well after the ion exchange reaction. It is worthy of notice that many nanoparticles can be seen in Figure 1e. It is speculated that these nanoparticles may composed with NiCo₂S₄, Ni₃S₂ and CDs. Hence, high-resolution TEM (HRTEM) measurement was performed to further confirm the above speculation. As shown in Figure 1f, it can be seen that the material has five different lattice spacings: 0.24, 0.28, 0.23, 0.24 and 0.22 nm, which are corresponding to the (400) lattice plane and (311) lattice plane of cubic NiCo₂S₄ phase, the (021) lattice plane and (003) lattice plane of the hexagonal Ni₃S₂, and the (100) lattice plane of the CDs, respectively. In addition, the 90° angle between the lattices corresponds well to the theoretical value of the cubic structure of NiCo₂S₄, and the 70.7° angle in the Ni₃S₂ structure corresponds to the theoretical value of (021) lattice plane.³² As it is described, in the CD/Ni₃S₂ system, the introduction of Co atoms can form a new NiCo₂S₄ phase, changing the electronic state of S in the original system. The CDs in the system in turn can affect the electronic state of Co (Figure S7a,b). The interaction between the electrons causes a synergistic effect between the phases of CDs, Ni₃S₂ and NiCo₂S₄, so that the performance of the catalyst can be significantly improved.

In addition, in HRTEM (Figure S4), the lattice fringe with the spacing of 0.22 nm is the (100) lattice plane of CDs, which fully proves the successfully doping of CDs. Element mapping images (Figure 1g) show that Ni, Co, S, C and other elements were uniformly distributed in the nanorods structure of the material. This also proves that nanorods consist of NiCo₂S₄,

Ni₃S₂ and CDs. Moreover, from Raman spectra (Figure S5), it further confirmed that CD/Ni₃S₂/NF were converted into CD/NiCo₂S₄/Ni₃S₂/NF after cation exchange reaction. The illustrated Raman spectra can be divided into two parts: spectra below 400 cm⁻¹ and spectra above 400 cm⁻¹. According to previously published literature, the group with a wavenumber region below 400 cm⁻¹ is the Raman spectral band of Ni₃S₂, and the group with a wavenumber region above 400 cm⁻¹ is Raman spectral band of NiCo₂S₄.³⁹ In addition, the peaks of the CDs were clearly observed at 1375 and 1600 cm⁻¹ (Figure S5b), which are corresponding to the D and G, respectively. These results clearly show that the obtained material contains NiCo₂S₄ and CD/Ni₃S₂. Besides, the Raman bands of NiCo₂S₄ were not observed in Raman spectra without cation exchange, indicating that the CD/NiCo₂S₄/Ni₃S₂/NF was successfully synthesized via cation exchange.

The XPS survey spectra of the pristine CD/NiCo₂S₄/Ni₃S₂/NF nanorods indicate the existence of Ni, Co, S and C, N, O. In the Ni 2p spectrum (Figure S6a), the appreciable fitting peaks at 853.2, 872.6 eV and 856.2, 874.4 eV are ascribed to Ni²⁺ and Ni³⁺, respectively. The satellite peaks at 861.2 and 879.2 eV, which are due to shakeup peaks of nickel. Similarly, Figure S6b shows that spin–orbit splitting values of Co 2p_{1/2} at 15.1 eV and Co 2p_{3/2} at 16.3 eV are ascribed to Co³⁺ and Co²⁺, respectively.⁴⁰ These results demonstrate the presence of NiCo₂S₄. In the case of S 2p spectrum (Figure S6c), the strongly fitting peaks centered at 162.0 and 163.2 eV are assigned to S 2p_{3/2} and S 2p_{1/2}, respectively.^{19,26,40} In detail, the peak at 163.2 eV is originated from the sulfur–metal bonds and the binding energy at 162.0 eV is attributed to S²⁻ in low coordination at the surface. In addition, S 2p fitting peaks centered at 168.9 eV is attributed to the surface sulfur species at certain higher oxidation states. The XPS spectra of C 1s (Figure S6d), N 1s (Figure S6e) and O 1s (Figure S6f)

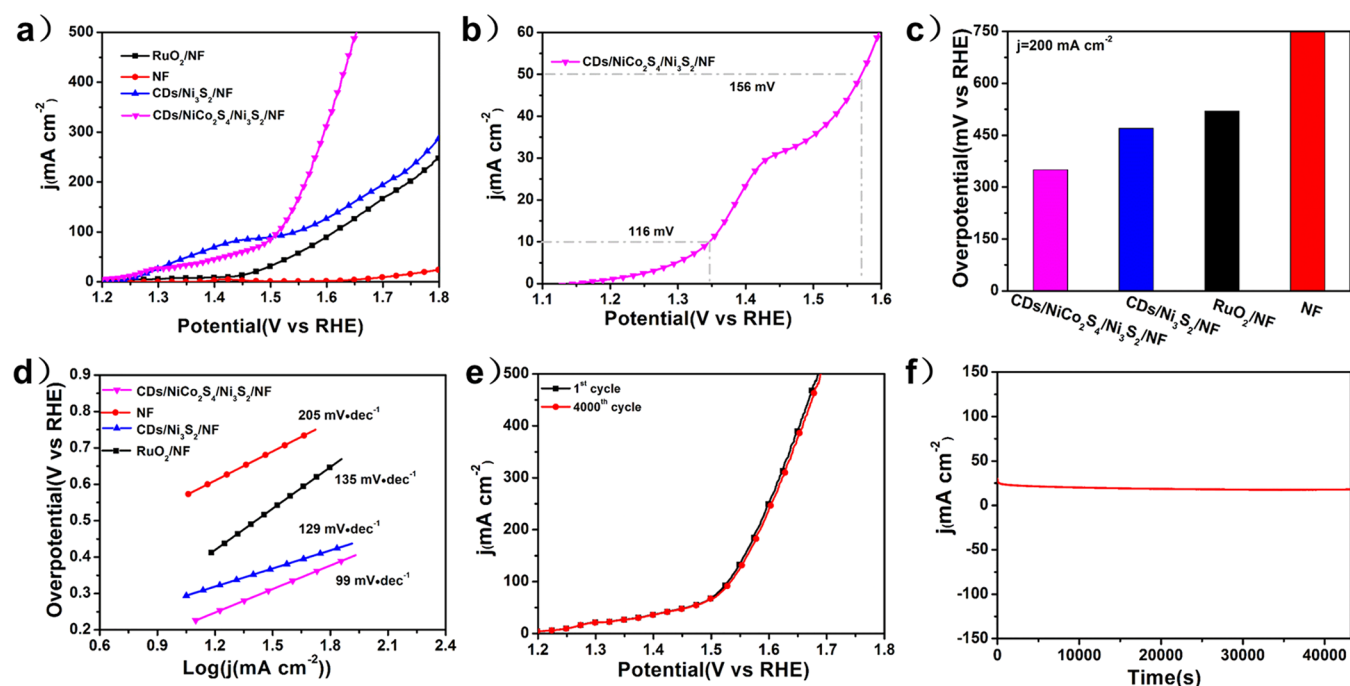


Figure 3. (a) LSV curves of CDs/NiCo₂S₄/Ni₃S₂/NF, CDs/Ni₃S₂/NF, bare Ni foam and RuO₂/NF. (b) LSV curve of CDs/NiCo₂S₄/Ni₃S₂/NF. (c) Overpotential histogram of CDs/NiCo₂S₄/Ni₃S₂/NF, CDs/Ni₃S₂/NF, bare Ni foam and RuO₂/NF. (d) Tafel plots of CDs/NiCo₂S₄/Ni₃S₂/NF, CDs/Ni₃S₂/NF, bare Ni foam and RuO₂/NF. (e) LSV curves for CDs/NiCo₂S₄/Ni₃S₂/NF before and after potential sweeps between 1.2 and 1.8 V for 4000 cycles. (f) 12 h chronoamperometry (at a static overpotential of 170 mV) of CDs/NiCo₂S₄/Ni₃S₂/NF.

confirm the successful introduction of CDs in the CDs/NiCo₂S₄/Ni₃S₂/NF system. All the above analytical results suggest that CDs/NiCo₂S₄/Ni₃S₂/NF was successfully synthesized.

CDs/NiCo₂S₄/Ni₃S₂/NF toward HER and Mechanism.

The HER performance test of CDs/NiCo₂S₄/Ni₃S₂/NF was conducted in a 1.0 M KOH electrolyte in a three-electrode system. CDs/NiCo₂S₄/Ni₃S₂/NF as self-supporting electrodes can be directly used as working electrodes in this system. By contrast, we also tested the performance of bare Ni foam, Pt/C on Ni foam (Pt-C/NF) and CDs/Ni₃S₂/NF under the same conditions. In Figure 2a, it can be seen that CDs/NiCo₂S₄/Ni₃S₂/NF electrode shows excellent HER performance, requiring the overpotential of only 127 mV to achieve the 10 mA cm⁻² current density. However, for bare Ni foam and CDs/Ni₃S₂/NF, it took the overpotentials of 247 and 187 mV to achieve the same current density. CDs/NiCo₂S₄/Ni₃S₂/NF have a rather low overpotential compared to the non-noble bifunctional electrocatalytic materials previously reported (Table S1).

The Tafel slopes of CDs/NiCo₂S₄/Ni₃S₂/NF, CDs/Ni₃S₂/NF, bare Ni foam and Pt-C/NF are 148, 155, 164 and 57 mV dec⁻¹, respectively (Figure 2d). This phenomenon indicates that the Volmer reaction is a rate-limiting step in the HER process. The stability of CDs/NiCo₂S₄/Ni₃S₂/NF was tested by a 4000 CV cycles polarization test at a voltage of 0 and -0.6 V (Figure 2e). What was interesting was that after 4000 cycles, the performance of HER was even improved. This is because a small amount of high valence Ni and Co can be randomly reduced to metal Ni and Co (Figure. S13). In this way, the conductivity and electron transfer rate of CDs/NiCo₂S₄/Ni₃S₂/NF can be improved. During stability testing, a 12 h stability test was performed (at a static overpotential of 127 mV). From the stability test, the CDs/NiCo₂S₄/Ni₃S₂/NF

shows a good stability with almost no large fluctuation in current density. Additionally, the morphology of CDs/NiCo₂S₄/Ni₃S₂/NF was basically unchanged after the HER stability test by the characterization of XRD pattern (Figure. S8a) and SEM image (Figure. S8b).

It can also be seen in Figure 2a that the hydrogen evolution potential of CDs/NiCo₂S₄/Ni₃S₂/NF is second only to the Pt-C/NF electrode. Such good performance may be attributed to the synergistic effect of the Ni and Co metal ions produced by the reduction of CDs/NiCo₂S₄/Ni₃S₂/NF nanoclusters. The specific mechanism of HER follows two reactions: $M + H_2O + e^- \rightarrow M-H_{ads} + OH^-$ (Volmer step) and $H_2O + M-H_{ads} + e^- \rightarrow H_2 + M + OH^-$ (Heyrovsky step).³ Through the optimization of these two processes, the catalyst can show highly efficient catalytic performance. According to the related study, it is known that one of the major challenges of using transition metal sulfides in the HER reaction is the formation of strong S-H bonds on the surface of the catalyst, which severely inhibits the reaction rate of HER.^{41,42} Therefore, for the Ni₃S₂ system introduced in this paper, the adsorption and desorption of H can be balanced by the introduction of Co atoms and CDs (Figure S7d). The electron interaction among Ni₃S₂, Co and CDs in the CDs/NiCo₂S₄/Ni₃S₂/NF can weaken the S-H_{ads} bond formed on the surface of the catalyst, which favors the desorption of H and promotes the Heyrovsky reaction. If only Ni₃S₂ is used as a catalyst, H_{ads} can be stably and easily adsorbed on the surface of catalyst. However, an excessively stable S-H_{ads} can make the transfer of H_{ads} to H₂ difficult, leading to low electrocatalytic activity.¹⁶⁻²³ This phenomenon can be demonstrated in the analysis of XPS (Figure S7c). It can be seen that after the doping with Co, the peaks of S 2p_{1/2} and S 2p_{3/2} of CDs/NiCo₂S₄/Ni₃S₂/NF demonstrate negative shifts of 0.24 and 0.21 eV, respectively. In addition, it can also be seen from

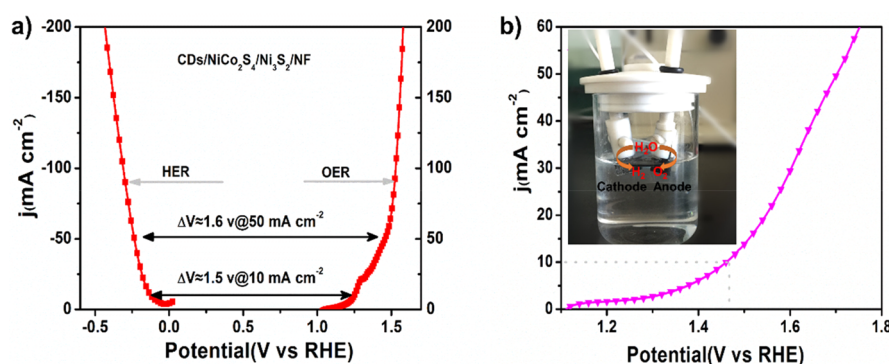


Figure 4. (a) Steady-state polarization curves of CDs/NiCo₂S₄/Ni₃S₂/NF in 1 M KOH for HER and OER. (b) LSV polarization curve of bifunctional CDs/NiCo₂S₄/Ni₃S₂/NF for overall water splitting. The inset is an optical photograph during the measurements.

Figure S7a that, compared to the system without carbon dots, the binding energy of Co atoms had a negative shift of 0.5 eV, indicating that after the Co atoms were incorporated into the system, they were in turn affected by the CDs. This can result in downshift of their d-band center and the optimization of key descriptor for HER performance (ΔG_{H}),^{43–45} contributing to the catalytic activity for HER. This phenomenon can also be demonstrated in the performance analysis of control experiments (Figure S14a). In addition, the Raman spectra (Figure S7d) can prove that the introduction of Co atoms and carbon dots in the Ni₃S₂ system can balance the adsorption and desorption of H. When the HER reaction at the potential of -127 mV vs RHE for 10 h were completed, a peak at about 2562 cm⁻¹ was detected for Ni₃S₂/NF, and a peak about 2500 cm⁻¹ was shown for CDs/NiCo₂S₄/Ni₃S₂/NF. These peaks were in line with S–H_{ads} bonds formed on the catalysts during HER.⁵¹ Compared with that of Ni₃S₂/NF (2562 cm⁻¹), Raman shift of S–H_{ads} for CDs/NiCo₂S₄/Ni₃S₂/NF (2500 cm⁻¹) was about 62 cm⁻¹ red-shifted, which showed that the S–H_{ads} bonds on CDs/NiCo₂S₄/Ni₃S₂/NF were weaker than those on Ni₃S₂/NF.

CDs/NiCo₂S₄/Ni₃S₂/NF toward OER and Mechanism. The OER performance test was conducted in a 1.0 M KOH electrolyte and a CDs/NiCo₂S₄/Ni₃S₂/NF being a self-supporting electrode. Similar measurements for RuO₂ modified NF (RuO₂/NF), bare nickel foam, and CDs/Ni₃S₂/NF were also conducted during the controllable experiments. It can be seen from Figure 3a that CDs/NiCo₂S₄/Ni₃S₂/NF exhibited the best catalytic activity. Before voltage reached 1.5 V, its current density was slightly lower than that of CDs/Ni₃S₂/NF. This is due to the voltage reached 1.5 V, a large amount of Ni^{II} oxidation of CDs/Ni₃S₂/NF can be converted into Ni^{III},³⁷ and there would be a clear oxidation peak, resulting in the sharp rise of current density. However, after the voltage exceeded 1.5 V, its current density was much higher than that of other materials.

As shown in Figure 3b, CDs/NiCo₂S₄/Ni₃S₂/NF only requires the overpotentials of 116 and 156 mV for the achievement of the current densities of 10 and 50 mA cm⁻², making it obviously better than other catalysts. It can also be proved in Figures 3c that its catalytic performance is also the best under high current. The performance of this catalyst is much better compared with the most currently reported electrocatalysts (Table S1). The OER kinetics was tested by corresponding Tafel plots (η versus $\log(j)$) of these electrodes (Figure 3d). The Tafel slope of CDs/NiCo₂S₄/Ni₃S₂/NF was 99 mV dec⁻¹. This was significantly lower than the Tafel slopes

of CDs/Ni₃S₂/NF (129 mV dec⁻¹), bare NF (206 mV dec⁻¹) and RuO₂/NF (135 mV dec⁻¹), showing that CDs/NiCo₂S₄/Ni₃S₂/NF had a faster OER rate. The stability of CDs/NiCo₂S₄/Ni₃S₂/NF showed no significant change after 4000 CV cycles polarization tests (Figure 3e). After a 12 h galvanostatic test (Figure 3f), no large attenuation was found, which indicated that this catalyst had a good stability. After the long OER test, the nanorods structure of CDs/NiCo₂S₄/Ni₃S₂/NF was only slightly changed by the XRD pattern and SEM characterization (Figure S9).

CDs/NiCo₂S₄/Ni₃S₂/NF catalyst exhibited such superior OER performance probably because of the synergistic effect of Co, CDs and Ni foam. In general, at the beginning of the OER, OH⁻ anions were adsorbed and discharged on the surface of catalyst in order to construct the adsorbed OH species. After that, OH⁻ had reaction with the adsorbed OH species, producing adsorbed atom O as well as H₂O, and releasing electron. Next, reaction of the adsorbed atom O and OH⁻ was taken place to form the adsorbed OOH species. After that, the OOH species would react with another OH⁻. In this way, adsorbed O₂ can be formed and another electron can be released. Finally, the adsorbed O₂ desorbed^{1,3,8} from the surface of the catalyst (Figure S10). In OER, the process in which the adsorbed OOH species were formed was considered as the rate-limiting step.⁴⁶ Moreover, the OER activity of transition metal materials depends on the interaction of the adsorbed OOH species with the 3d orbital of transition metals.^{47,48} There are also studies proving that the increase in 3d orbital electron density in Co-based OER catalysts favors the construction of the adsorbed OOH species, which can then help to increase the OER activity.^{49–53} The doping of Co in CDs/Ni₃S₂/NF catalyst reduced the 2p_{3/2} binding energy of Ni atoms (Figure S7b), reflecting that the doping of Co atoms can reduce the binding energy of Ni atoms and enable Ni atoms. In this way, more electrons can be obtained. In addition, compared with the carbonless system, the binding energy of Co atoms also has a negative shift of 0.5 eV (Figure S7a), which indicates that there are more electrons in the 3d orbital of Co atoms. This is beneficial to the construction of OOH species. At the same time, this can help to promote the OER. This phenomenon can also be demonstrated in the performance analysis of control experiments (Figure S14b).

CDs/NiCo₂S₄/Ni₃S₂/NF toward Overall Water Splitting. Figure 4a shows the water splitting curve for HER and OER tests in 1 M KOH solution. The overpotential of 1.5 V can produce the current density to 10 mA cm⁻². An electrolyzer using CDs/NiCo₂S₄/Ni₃S₂/NF as both cathode

and anode was assembled for overall water splitting. The CDs/ $\text{NiCo}_2\text{S}_4/\text{Ni}_3\text{S}_2/\text{NF}$ electrodes showed great stability for the electrolytic reaction for 12 h (Figure 4b). All these show that the catalytic performance of CDs/ $\text{NiCo}_2\text{S}_4/\text{Ni}_3\text{S}_2/\text{NF}$ is better than most of the reported bifunctional electrocatalysts for overall water splitting (Table S1).

The reasons why CDs/ $\text{NiCo}_2\text{S}_4/\text{Ni}_3\text{S}_2/\text{NF}$ can have such excellent performance for overall water splitting are that (1) NiCo_2S_4 and Ni_3S_2 are metal sulfides with good conductivity because they have Ni–Ni bonds. (2) A large number of exposed active sites provided by carbon dots modified transition metal chalcogenide (Ni_3S_2 and NiCo_2S_4) and the CDs/ $\text{Ni}_3\text{S}_2/\text{NF}$ precursors have good stability and can fully retain their active sites, which is beneficial to improve the catalytic performance. (3) The strong interfacial interaction at CDs/ $\text{NiCo}_2\text{S}_4/\text{Ni}_3\text{S}_2/\text{NF}$ heterojunction interfaces with the strengthened H binding. Therefore, further introduction of a catalytically active phase (NiCo_2S_4) on the basis of the full play of the advantages of the precursor CDs/ $\text{Ni}_3\text{S}_2/\text{NF}$ can change the electronic structure of S in precursor, balance the absorption and desorption of H in catalytic process, and achieve higher electrochemical active area (Figure S11) and increases the fast charge transfer pathways (Figure S12).

CONCLUSIONS

To sum up, a noble-metal-free and self-standing CDs/ $\text{NiCo}_2\text{S}_4/\text{Ni}_3\text{S}_2/\text{NF}$ electrode was constructed successfully by a facile hydrothermal treatment and subsequent ion exchange process. As a catalyst of water splitting, CDs/ $\text{NiCo}_2\text{S}_4/\text{Ni}_3\text{S}_2/\text{NF}$ shows excellent electrocatalytic performance compared to reported non-noble metal-free catalysts, and about 1.50 V can drive the overall water splitting with superior durability. The reason why CDs/ $\text{NiCo}_2\text{S}_4/\text{Ni}_3\text{S}_2/\text{NF}$ can have such superior electrocatalytic performance is that there are a great number of active sites, the synergy between carbon dots and transition metal sulfides, and the good conductivity of the substrate. In this work, cation exchange for heteroatom doping provides a new reliable method for developing transition metal sulfide electrocatalysts. Hence, the researchers in the fields of electrocatalysis, photocatalysis, energy storage and conversion, etc. also have interest in this work.

ASSOCIATED CONTENT

Supporting Information

The Supporting Information is available free of charge on the ACS Publications website at DOI: 10.1021/acssuschemeng.8b05611.

SEM, TEM and HRTEM; XRD, Raman and XPS; cyclic voltammetry curves and EIS; comparison of water splitting performance (PDF)

AUTHOR INFORMATION

Corresponding Author

*M. Wu. E-mail address: wumb@upc.edu.cn.

ORCID

Hui Liu: 0000-0001-7815-4200

Yuan Rao: 0000-0002-6770-6230

Mingbo Wu: 0000-0003-0048-778X

Notes

The authors declare no competing financial interest.

ACKNOWLEDGMENTS

This work was financially supported by the National Natural Science Foundation of China (Nos. 51572296, U1662113, 51372277); the Fundamental Research Funds for the Central Universities of China (Nos. 15CX08005A, 14CX02127A, 17CX06029); the Financial Support from Taishan Scholar Project, and Scientific Research and Technology Development Project of Petrochina Co., LTD (2016B-2004(GF)).

REFERENCES

- (1) Faber, M. S.; Jin, S. Earth-abundant Inorganic Electrocatalysts and Their Nanostructures for Energy Conversion Applications. *Energy Environ. Sci.* **2014**, *7* (11), 3519–3542.
- (2) Turner, J. A. Sustainable Hydrogen Production. *Science* **2004**, *305* (5686), 972–974.
- (3) Seh, Z. W.; Kibsgaard, J.; Dickens, C. F.; Chorkendorff, I.; Norskov, J. K.; Jaramillo, T. F. Combining Theory and Experiment in Electrocatalysis: Insights into Materials Design. *Science* **2017**, *355* (6321), No. eaad4998.
- (4) Wang, J.; Cui, W.; Liu, Q.; Xing, Z.; Asiri, A. M.; Sun, X. Recent Progress in Cobalt-Based Heterogeneous Catalysts for Electrochemical Water Splitting. *Adv. Mater.* **2016**, *28* (2), 215–230.
- (5) Suntivich, J.; May, K. J.; Gasteiger, H. A.; Goodenough, J. B.; Shao-Horn, Y. A Perovskite Oxide Optimized for Oxygen Evolution Catalysis from Molecular Orbital Principles. *Science* **2011**, *334* (6061), 1383.
- (6) Kanan, M. W.; Nocera, D. G. In Situ Formation of an Oxygen-Evolving Catalyst in Neutral Water Containing Phosphate and Co^{2+} . *Science* **2008**, *321* (5892), 1072–1075.
- (7) Fang, B.; Kim, J. H.; Yu, J.-S. Colloid-imprinted Carbon with Superb Nanostructure as An Efficient Cathode Electrocatalyst Support in Proton Exchange Membrane Fuel Cell. *Electrochem. Commun.* **2008**, *10* (4), 659–662.
- (8) Zou, X.; Zhang, Y. Noble Metal-free Hydrogen Evolution Catalysts for Water Splitting. *Chem. Soc. Rev.* **2015**, *44* (15), 5148–5180.
- (9) Chen, P.; Xu, K.; Fang, Z.; Tong, Y.; Wu, J.; Lu, X.; Peng, X.; Ding, H.; Wu, C.; Xie, Y. Metallic Co_4N Porous Nanowire Arrays Activated by Surface Oxidation as Electrocatalysts for the Oxygen Evolution Reaction. *Angew. Chem.* **2015**, *127* (49), 14923–14927.
- (10) Zhuang, L.; Ge, L.; Yang, Y.; Li, M.; Jia, Y.; Yao, X.; Zhu, Z. Ultrathin Iron-Cobalt Oxide Nanosheets with Abundant Oxygen Vacancies for the Oxygen Evolution Reaction. *Adv. Mater.* **2017**, *29* (17), 1606793.
- (11) Luo, J.; Im, J.-H.; Mayer, M. T.; Schreiber, M.; Nazeeruddin, M. K.; Park, N.-G.; Tilley, S. D.; Fan, H. J.; Grätzel, M. Water Photolysis at 12.3% Efficiency via Perovskite Photovoltaics and Earth-abundant Catalysts. *Science* **2014**, *345* (6204), 1593.
- (12) Jin, Y.; Wang, H.; Li, J.; Yue, X.; Han, Y.; Shen, P. K.; Cui, Y. Porous MoO_2 Nanosheets as Non-noble Bifunctional Electrocatalysts for Overall Water Splitting. *Adv. Mater.* **2016**, *28* (19), 3785–3790.
- (13) Li, J.; Wang, Y.; Zhou, T.; Zhang, H.; Sun, X.; Tang, J.; Zhang, L.; Al-Enizi, A. M.; Yang, Z.; Zheng, G. Nanoparticle Superlattices as Efficient Bifunctional Electrocatalysts for Water Splitting. *J. Am. Chem. Soc.* **2015**, *137* (45), 14305–14312.
- (14) Jia, X.; Zhao, Y.; Chen, G.; Shang, L.; Shi, R.; Kang, X.; Waterhouse, G. I. N.; Wu, L.-Z.; Tung, C.-H.; Zhang, T. Ni_3FeN Nanoparticles Derived from Ultrathin NiFe -Layered Double Hydroxide Nanosheets: An Efficient Overall Water Splitting Electrocatalyst. *Adv. Energy Mater.* **2016**, *6* (10), 1502585.
- (15) Zhang, Q.; Wang, Y.; Wang, Y.; Al-Enizi, A. M.; Elzatahy, A. A.; Zheng, G. Myriophyllum-like Hierarchical $\text{TiN}@\text{Ni}_3\text{N}$ Nanowire Arrays for Bifunctional Water Splitting Catalysts. *J. Mater. Chem. A* **2016**, *4* (15), 5713–5718.
- (16) Li, H.; Tsai, C.; Koh, A. L.; Cai, L.; Contryman, A. W.; Fragapane, A. H.; Zhao, J.; Han, H. S.; Manoharan, H. C.; Abild-Pedersen, F.; Norskov, J. K.; Zheng, X. Corrigendum: Activating and Optimizing MoS_2 Basal Planes for Hydrogen Evolution through The

Formation of Strained Sulphur Vacancies. *Nat. Mater.* **2016**, *15* (1), 48–53.

(17) Pramoda, K.; Gupta, U.; Chhetri, M.; Bandyopadhyay, A.; Pati, S. K.; Rao, C. N. Nanocomposites of C_3N_4 with Layers of MoS_2 and Nitrogenated RGO, Obtained by Covalent Cross-Linking: Synthesis, Characterization, and HER Activity. *ACS Appl. Mater. Interfaces* **2017**, *9* (12), 10664–10672.

(18) Yang, L.; Zhou, W.; Lu, J.; Hou, D.; Ke, Y.; Li, G.; Tang, Z.; Kang, X.; Chen, S. Hierarchical Spheres Constructed by Defect-rich MoS_2 /Carbon Nanosheets for Efficient Electrocatalytic Hydrogen Evolution. *Nano Energy* **2016**, *22*, 490–498.

(19) Feng, L.; Yu, G.; Wu, Y.; Li, G. D.; Li, H.; Sun, Y.; Asefa, T.; Chen, W.; Zou, X. High-index Faceted Ni_3S_2 Nanosheet Arrays as Highly Active and Ultrastable Electrocatalysts for Water Splitting. *J. Am. Chem. Soc.* **2015**, *137* (44), 14023–14026.

(20) Ouyang, C.; Wang, X.; Wang, C.; Zhang, X.; Wu, J.; Ma, Z.; Dou, S.; Wang, S. Hierarchically Porous Ni_3S_2 Nanorod Array Foam as Highly Efficient Electrocatalyst for Hydrogen Evolution Reaction and Oxygen Evolution Reaction. *Electrochim. Acta* **2015**, *174*, 297–301.

(21) Jiang, N.; Tang, Q.; Sheng, M.; You, B.; Jiang, D.-e.; Sun, Y. Nickel Sulfides for Electrocatalytic Hydrogen Evolution Under Alkaline Conditions: A Case Study of Crystalline NiS , NiS_2 , and Ni_3S_2 Nanoparticles. *Catal. Sci. Technol.* **2016**, *6* (4), 1077–1084.

(22) Wang, X.; Liu, R.; Zhang, Y.; Zeng, L.; Liu, A. Hierarchical Ni_3S_2 - $NiOOH$ Hetero-nanocomposite Grown on Nickel Foam as a Noble-metal-free Electrocatalyst for Hydrogen Evolution Reaction in Alkaline Electrolyte. *Appl. Surf. Sci.* **2018**, *456*, 164–173.

(23) Ren, J.-T.; Yuan, Z.-Y. Hierarchical Nickel Sulfide Nanosheets Directly Grown on Ni Foam: A Stable and Efficient Electrocatalyst for Water Reduction and Oxidation in Alkaline Medium. *ACS Sustainable Chem. Eng.* **2017**, *5* (8), 7203–7210.

(24) Yin, Y.; Zhang, Y.; Gao, T.; Yao, T.; Zhang, X.; Han, J.; Wang, X.; Zhang, Z.; Xu, P.; Zhang, P.; Cao, X.; Song, B.; Jin, S. Synergistic Phase and Disorder Engineering in 1T- $MoSe_2$ Nanosheets for Enhanced Hydrogen-Evolution Reaction. *Adv. Mater.* **2017**, *29* (28), 1700311.

(25) Liu, B.; Zhao, Y.; Peng, H.; Zhang, Z.; Sit, C. K.; Yuen, M.; Zhang, T.; Lee, C.; Zhang, W. Nickel-Cobalt Diselenide 3D Mesoporous Nanosheet Networks Supported on Ni Foam: An All-pH Highly Efficient Integrated Electrocatalyst for Hydrogen Evolution. *Adv. Mater.* **2017**, *29*, 1606521.

(26) Liu, D.; Lu, Q.; Luo, Y.; Sun, X.; Asiri, A. M. $NiCo_2S_4$ Nanowires Array as An Efficient Bifunctional Electrocatalyst for Full Water Splitting with Superior Activity. *Nanoscale* **2015**, *7* (37), 15122–15126.

(27) Liu, J.; Wang, J.; Zhang, B.; Ruan, Y.; Lv, L.; Ji, X.; Xu, K.; Miao, L.; Jiang, J. Hierarchical $NiCo_2S_4$ @ $NiFe$ LDH Heterostructures Supported on Nickel Foam for Enhanced Overall-Water-Splitting Activity. *ACS Appl. Mater. Interfaces* **2017**, *9* (18), 15364–15372.

(28) Sivanantham, A.; Ganesan, P.; Shanmugam, S. Hierarchical $NiCo_2S_4$ Nanowire Arrays Supported on Ni Foam: An Efficient and Durable Bifunctional Electrocatalyst for Oxygen and Hydrogen Evolution Reactions. *Adv. Funct. Mater.* **2016**, *26* (26), 4661–4672.

(29) Qu, Y.; Yang, M.; Chai, J.; Tang, Z.; Shao, M.; Kwok, C. T.; Yang, M.; Wang, Z.; Chua, D.; Wang, S.; Lu, Z.; Pan, H. Facile Synthesis of Vanadium-Doped Ni_3S_2 Nanowire Arrays as Active Electrocatalyst for Hydrogen Evolution Reaction. *ACS Appl. Mater. Interfaces* **2017**, *9* (7), S959–S967.

(30) Yang, Y.; Zhang, K.; Lin, H.; Li, X.; Chan, H. C.; Yang, L.; Gao, Q. MoS_2 - Ni_3S_2 Heteronanorods as Efficient and Stable Bifunctional Electrocatalysts for Overall Water Splitting. *ACS Catal.* **2017**, *7* (4), 2357–2366.

(31) Zhang, J.; Wang, T.; Pohl, D.; Rellinghaus, B.; Dong, R.; Liu, S.; Zhuang, X.; Feng, X. Interface Engineering of MoS_2 / Ni_3S_2 Heterostructures for Highly Enhanced Electrochemical Overall-Water-Splitting Activity. *Angew. Chem.* **2016**, *128* (23), 6814–6819.

(32) Wu, Y.; Liu, Y.; Li, G.-D.; Zou, X.; Lian, X.; Wang, D.; Sun, L.; Asefa, T.; Zou, X. Efficient Electrocatalysis of Overall Water Splitting

by Ultrasmall $Ni_xCo_{3-x}S_4$ Coupled Ni_3S_2 Nanosheet Arrays. *Nano Energy* **2017**, *35*, 161–170.

(33) Zhang, Y.; Rui, K.; Ma, Z.; Sun, W.; Wang, Q.; Wu, P.; Zhang, Q.; Li, D.; Du, M.; Zhang, W.; Lin, H.; Zhu, J. Cost-Effective Vertical Carbon Nanosheets/Iron-Based Composites as Efficient Electrocatalysts for Water Splitting Reaction. *Chem. Mater.* **2018**, *30* (14), 4762–4769.

(34) Yu, C.; Liu, Z.; Han, X.; Huang, H.; Zhao, C.; Yang, J.; Qiu, J. NiCo-layered double hydroxides vertically assembled on carbon fiber papers as binder-free high-active electrocatalysts for water oxidation. *Carbon* **2016**, *110*, 1–7.

(35) Ritter, K. A.; Lyding, J. W. The influence of edge structure on the electronic properties of graphene quantum dots and nanoribbons. *Nat. Mater.* **2009**, *8* (3), 235–242.

(36) Zhang, Z.; Zhang, J.; Chen, N.; Qu, L. Graphene quantum dots: an emerging material for energy-related applications and beyond. *Energy Environ. Sci.* **2012**, *5* (10), 8869–8890.

(37) Rao, Y.; Ning, H.; Ma, X.; Liu, Y.; Wang, Y.; Liu, H.; Liu, J.; Zhao, Q.; Wu, M. Template-free Synthesis of Coral-like Nitrogen-doped Carbon Dots/ Ni_3S_2 / Ni Foam Composites as Highly Efficient Electrodes for Water Splitting. *Carbon* **2018**, *129*, 335–341.

(38) Beberwyck, B. J.; Surendranath, Y.; Alivisatos, A. P. Cation Exchange: A Versatile Tool for Nanomaterials Synthesis. *J. Phys. Chem. C* **2013**, *117* (39), 19759–19770.

(39) Xia, C.; Li, P.; Gandi, A. N.; Schwingenschlöggl, U.; Alshareef, H. N. Is $NiCo_2S_4$ Really a Semiconductor? *Chem. Mater.* **2015**, *27* (19), 6482–6485.

(40) He, W.; Wang, C.; Li, H.; Deng, X.; Xu, X.; Zhai, T. Ultrathin and Porous Ni_3S_2 / $CoNi_2S_4$ 3D-Network Structure for Superhigh Energy Density Asymmetric Supercapacitors. *Adv. Energy Mater.* **2017**, *7* (21), 1700983.

(41) Zhou, W.; Wu, X.-J.; Cao, X.; Huang, X.; Tan, C.; Tian, J.; Liu, H.; Wang, J.; Zhang, H. Ni_3S_2 Nanorods/ Ni Foam Composite Electrode with Low Overpotential for Electrocatalytic Oxygen Evolution. *Energy Environ. Sci.* **2013**, *6* (10), 2921–2924.

(42) Zhu, H.; Zhang, J.; Yanzhang, R.; Du, M.; Wang, Q.; Gao, G.; Wu, J.; Wu, G.; Zhang, M.; Liu, B.; Yao, J.; Zhang, X. When Cubic Cobalt Sulfide Meets Layered Molybdenum Disulfide: A Core-shell System Toward Synergetic Electrocatalytic Water Splitting. *Adv. Mater.* **2015**, *27* (32), 4752–4759.

(43) Zhang, R.; Tang, C.; Kong, R.; Du, G.; Asiri, A. M.; Chen, L.; Sun, X. Al-Doped CoP Nanoarray: A Durable Water-splitting Electrocatalyst with Superhigh Activity. *Nanoscale* **2017**, *9* (14), 4793–4800.

(44) Tang, C.; Zhang, R.; Lu, W.; He, L.; Jiang, X.; Asiri, A. M.; Sun, X. Fe-Doped CoP Nanoarray: A Monolithic Multifunctional Catalyst for Highly Efficient Hydrogen Generation. *Adv. Mater.* **2017**, *29* (2), 1602441.

(45) Tang, C.; Gan, L.; Zhang, R.; Lu, W.; Jiang, X.; Asiri, A. M.; Sun, X.; Wang, J.; Chen, L. Ternary $Fe_xCo_{1-x}P$ Nanowire Array as a Robust Hydrogen Evolution Reaction Electrocatalyst with Pt-like Activity: Experimental and Theoretical Insight. *Nano Lett.* **2016**, *16* (10), 6617–6621.

(46) Yeo, B. S.; Bell, A. T. Enhanced Activity of Gold-supported Cobalt Oxide for The Electrochemical Evolution of Oxygen. *J. Am. Chem. Soc.* **2011**, *133* (14), 5587–5593.

(47) Grimaud, A.; May, K. J.; Carlton, C. E.; Lee, Y. L.; Risch, M.; Hong, W. T.; Zhou, J.; Shao-Horn, Y. Double Perovskites as A Family of Highly Active Catalysts for Oxygen Evolution in Alkaline Solution. *Nat. Commun.* **2013**, *4*, 2439.

(48) Han, X.; Yu, C.; Zhou, S.; Zhao, C.; Huang, H.; Yang, J.; Liu, Z.; Zhao, J.; Qiu, J. Ultrasensitive Iron-Triggered Nanosized Fe-CoOOH Integrated with Graphene for Highly Efficient Oxygen Evolution. *Adv. Energy Mater.* **2017**, *7* (14), 1602148.

(49) Zhao, S.; Jin, R.; Abroshan, H.; Zeng, C.; Zhang, H.; House, S. D.; Gottlieb, E.; Kim, H. J.; Yang, J. C.; Jin, R. Gold Nanoclusters Promote Electrocatalytic Water Oxidation at the Nanocluster/ $CoSe_2$ Interface. *J. Am. Chem. Soc.* **2017**, *139* (3), 1077–1080.

(50) Zheng, Y. R.; Gao, M. R.; Gao, Q.; Li, H. H.; Xu, J.; Wu, Z. Y.; Yu, S. H. An Efficient CeO₂ /CoSe₂ Nanobelt Composite for Electrochemical Water Oxidation. *Small* **2015**, *11* (2), 182–188.

(51) Deng, Y.; Ting, L. R. L.; Neo, P. H. L.; Zhang, Y.-J.; Peterson, A. A.; Yeo, B. S. Operando Raman Spectroscopy of Amorphous Molybdenum Sulfide (MoS_x) during the Electrochemical Hydrogen Evolution Reaction: Identification of Sulfur Atoms as Catalytically Active Sites for H⁺ Reduction. *ACS Catal.* **2016**, *6* (11), 7790–7798.

(52) Han, X.; Yu, C.; Yang, J.; Zhao, C.; Huang, H.; Liu, Z.; Ajayan, P.; Qiu, J. Mass and Charge Transfer Coenhanced Oxygen Evolution Behaviors in CoFe-Layered Double Hydroxide Assembled on Graphene. *Adv. Mater. Interfaces* **2016**, *3* (7), 1500782.

(53) Zhang, Y.; Zhou, Q.; Zhu, J.; et al. Nanostructured metal chalcogenides for energy storage and electrocatalysis. *Adv. Funct. Mater.* **2017**, *27* (35), 1702317.